Biophysical *Journal*
Article

Biophysical Society

Effect of an Intrinsically Disordered Plant Stress Protein on the Properties of Water

Luisa A. Ferreira,[1] Alicyia Walczyk Mooradally,[2] Boris Zaslavsky,[1,*] Vladimir N. Uversky,[3,4,*] and Steffen P. Graether[2,*]

[1]Cleveland Diagnostics, Cleveland, Ohio; [2]Department of Molecular and Cellular Biology, University of Guelph, Guelph, Ontario, Canada; [3]Department of Molecular Medicine and Byrd Alzheimer's Research Institute, Morsani College of Medicine, University of South Florida, Tampa, Florida; and [4]Institute for Biological Instrumentation, Russian Academy of Sciences, Pushchino, Moscow Region, Russian Federation

ABSTRACT Dehydrins are plant proteins that are able to protect plants from various forms of dehydrative stress such as drought, cold, and high salinity. Dehydrins can prevent enzymes from losing activity after freeze/thaw treatments. Previous studies had suggested that the dehydrins function by a molecular shield effect, essentially preventing a denatured enzyme from aggregating with another enzyme. Therefore, the larger the dehydrin, the larger the shield and theoretically the more effective the protection. Although this relationship holds for smaller dehydrins, it fails to explain why larger dehydrins are less efficient than would be predicted from their size. Using solvatochromic dyes to probe the solvent features of water, we first confirm that the dehydrins do not bind the dyes, which would interfere with interpretation of the data. We then show that the dehydrins have an effect on three solvent properties of water (dipolarity/polarizability, hydrogen-bond donor acidity and hydrogen-bond acceptor basicity), which can contribute to the protective mechanism of these proteins. Interpretation of these data suggests that although polyethylene glycol and dehydrins have similar protective effects, dehydrins may more efficiently modify the hydrogen-bonding ability of bulk water to prevent enzyme denaturation. This possibly explains why dehydrins recover slightly more enzyme activity than polyethylene glycol.

INTRODUCTION

Intrinsically disordered proteins (IDPs, also known as intrinsically unstructured or natively unfolded proteins) are a class of highly dynamic proteins without unique three-dimensional structures (1–5). IDPs can be identified through a variety of biophysical methods, such as NMR, circular dichroism, and size exclusion chromatography (6–8), or predicted through a number of bioinformatics methods, such as identifying clusters of amino acids with a high propensity for disorder (9) or estimating the contact energy of individual residues (10). The functional roles of IDPs are almost as diverse as their structure, though IDPs are particularly abundant in protein families involved in transcription and cell cycle control (1,2,11,12). Another emerging role for IDPs includes protecting cells from stress damage, such as aggregation, misfolding, and oxidative damage (13,14). One well-studied IDP family in this group is the family of plant dehydrins (dehydration proteins) (15–19).

Dehydrins were first identified as proteins in cotton seeds belonging to the late embryogenesis abundant protein family (20). Plants differ from animals, as they are sessile organisms; therefore, they need cellular and molecular defense mechanisms, such as late embryogenesis abundant proteins, to cope with various abiotic stresses such as drought, cold, and high salinity (21–23). Dehydrins are characterized by the presence of a lysine-rich motif known as the K-segment (24). Technically, the K-segment is best described as a position scoring matrix (25), but it also can be practically described as [XKXGXX(D/E)KIK(D/E)KXPG] (25), in which "X" represents any amino acid. The other two conserved motifs, which are not present in every dehydrin, are the S-segment [LHR(S/T)$GS_{4–6}$(S/D/E)$(D/E)_3$] (25) and the Y-segment [D(D/E)(Y/H/F)GNPX] (25). Several other conserved motifs have been identified in dehydrins as well (see, for example, (17,25–28)), though their ubiquity among all plants has not been fully established. In between the conserved segments are the ϕ-segments, which represent poorly conserved motifs of variable length (typically $<$50 residues) and a sequence composition bias toward smaller amino acids that are polar or charged. The roles of the segments are multifaceted and

Submitted July 23, 2018, and accepted for publication September 18, 2018.
*Correspondence: boris.zaslavsky@cleveland-diagnostics.com or vuversky@health.usf.edu or graether@uoguelph.ca
Editor: Amedeo Caflisch.
https://doi.org/10.1016/j.bpj.2018.09.014

under active investigation and will not be further described here.

The biological roles of dehydrins have been examined through several molecular biological approaches (29–31), typically based on the observation that the presence of dehydrins is correlated with a plant's ability to resist dehydrative stress damage. The exact in vivo role of dehydrins has not been fully elucidated; several clues, however, have come from in vitro studies. Some of the proposed functions of dehydrins include binding metal/ions to assist in reactive oxygen species scavenging, protecting against changes in membrane fluidity to preserve membrane function, and preventing the denaturation of metabolic enzymes at low temperatures (16,32–34). With respect to enzyme protection, the standard cryoprotection assay consists of freezing and thawing lactate dehydrogenase (LDH) multiple times using liquid nitrogen, followed by measuring the residual enzyme activity. Comparison of the ability of dehydrins to protect LDH in such freezing and thawing experiments is often done using the PD_{50} value, which represents the concentration of dehydrin or a control compound required to recover 50% of the original LDH activity. Hence, lower PD_{50} values represent more efficient protection.

Our previous work showed that the K_2 dehydrin prevents loss of LDH activity by averting enzyme aggregation (35) and that the hydrodynamic radius (R_h) of a dehydrin correlates with the PD_{50} value (36). We also showed that using polyethylene glycol (PEG) molecules of a similar R_h to the dehydrins results in similar PD_{50} values. One interpretation of these data illustrates that dehydrins function as a molecular shield by preventing damaged, aggregation-prone LDH from encountering other damaged LDH molecules (35,36). The shield, or more specifically the volume exclusion effect, represents the restricted accessible volume (i.e., the hard, steric interactions) in the presence of these protective compounds, such as dehydrins. The experimentally observed problem with this proposal is that the relationship between PD_{50} and R_h became asymptotic with the larger dehydrins (36). Clearly this interpretation is simplistic, and other factors such as the reduction of available volume to LDH, the concentration of the protective compounds, and the effect of the protective compounds on water must also be considered.

We examine here the effect of dehydrins on the solvent properties of water. Although the effect of dehydrins on the hydration surface at subzero temperatures has been previously reported (37), the possible effects of dehydrin on bulk water properties are unknown, and hence the need for this study. Other studies (38–40) have shown that the effects of various compounds on the solvent features of water can be determined using the solvatochromic comparison method (41–43). The solvatochromic comparison method—pioneered by Kamlet, Taft, and their co-workers (41–43)—is based on using dyes that respond to changes in the solvent properties by shifting positions (wavelengths) of their absorption maxima. The water soluble dyes used in this study are 4-nitroanisole, 4-nitrophenol, and Reichardt's $E_T(8)$ betaine dye (4-[2,6-diphenyl-4-(pyridin-4-yl)pyridinium-1-yl]-2,6-bis(pyridin-3-yl)phenolate betaine dye). Solute-solvent interactions include a variety of different interactions, such as dipole-dipole, hydrogen bonding, and electrostatic effects. To characterize the ability of various solvents to participate in these interactions, it has been suggested to use three different scales of solvent features (41–43). One scale characterizes the relative ability of solvents to participate in dipole-dipole interactions (dipolarity/polarizability scale, π^*) (43). Another scale describes the relative abilities of the different solvents to serve as acceptors of hydrogen bonds (HBA basicity scale, α), and the third scale characterizes the ability of solvents to donate hydrogen bonds (HBD acidity scale, β) (41,42). Various solvents are characterized on each scale according to the response they induce in a set of solvatochromic dyes. The response of a dye to its environment is represented by the position of the longest wavelength of the ultraviolet-visible (UV-vis) absorption band in a given solvent. It has been previously shown (44–47) that the solvent-dependent physicochemical properties of a solute in a given solvent may be described as a linear combination of the solvent's abilities to participate in various types of interactions with the solute multiplied by the solute-dependent coefficients, representing the contributions of the different types of interactions.

It should be noted that although the solvatochromic comparison method was originally developed for characterization of solute properties in various organic solvents, its application was recently extended to the analysis of ionic liquids (48), aqueous solutions of nonionic polymers (38,39,49), small organic compounds (39,50), and inorganic salts (40). It should also be noted that according to Rani et al. (48), the particular values of the responses of the solvatochromic dyes have no fundamental physical meaning in and of themselves and should instead be viewed as a relative estimate of the specific solvent features.

Among the over 40 various compounds that have been examined by this approach so far (38–40,51), only two were proteins: human heat shock protein 6B (HSPB6 (39)) and elastin-like polypeptide (ELP) with the $(GVGVP)_{40}$ sequence (51). Most proteins are prone to binding aromatic organic solvatochromic dyes, rendering the assay useless for them. It appears that IDPs, with their paucity of hydrophobic amino acids and general lack of a hydrophobic core, are good candidates for solvent property studies.

The purpose of this study is to examine effects of three different dehydrins on the solvent features of bulk water and see whether this effect can explain the limiting effect of dehydrin size on the enzyme cryoprotection.

MATERIALS AND METHODS

Proteins

The K_2, K_4, and K_{10} dehydrins were produced recombinantly in bacteria and purified as previously described (36). Because of the high protein concentrations and large number of samples required for these assays, 100 mg of each protein was purified from ~20 L of Lysogeny broth media.

Solvatochromic measurements

The solvatochromic probe 4-nitrophenol (spectrophotometric grade) was purchased from Sigma (St. Louis, MO). The 4-nitroanisole probe (>99%) was supplied by Acros Organic (Bridgewater, NJ). Reichardt's carboxylated betaine dye, sodium 2,6-diphenyl-4-[4-(4-carboxylatophenyl)-2,6-diphenylpyridinium-1-yl]phenolate, was synthesized according to the procedure reported previously (52).

All dehydrin solutions were prepared in deionized water. The solvatochromic probes 4-nitroanisole, 4-nitrophenol, and Reichardt's $E_T(8)$ betaine dye were used to determine the dipolarity/polarizability π^*, hydrogen bond acceptor (HBA) basicity β, and hydrogen bond donor (HBD) acidity α of the aqueous media in which the dehydrins were dissolved.

Aqueous solutions (~3–10 mM) of each solvatochromic dye were prepared, and 10–20 μL of each was added separately to a total volume of 500 μL of the dehydrin solution. A strong base was added to the samples (~5 μL of 1 M NaOH to 500 μL of the dehydrin solution) containing Reichardt's carboxylate-substituted betaine dye to ensure a basic pH. A strong acid (~10 μL of 1 M HCl to 500 μL of the solution) was added to the samples containing 4-nitrophenol to eliminate the charge-transfer UV-vis absorption bands of the phenolate anion that are observed in some solutions. The respective blank solutions without dye were prepared separately. The samples were mixed thoroughly in a vortex mixer, and the UV-vis absorption spectra of each solution were acquired. To check the reproducibility, possible aggregation, and specific interaction effects, the position of the band maximum in each sample was measured in three to five separate aliquots. A UV-Vis microplate reader spectrophotometer SpectraMax Plus384 (Molecular Devices, Sunnyvale, CA) with a bandwidth of 2.0 nm, data interval of 1 nm, and high-resolution scan (~0.5 nm/s) was used for acquisition of the UV-Vis molecular absorbance data. The absorption spectra of the probes were determined over the spectral range from 240 to 600 nm in each solution. Pure dehydrin solutions containing no dye (blank) were scanned first to establish a baseline. The wavelength of maximal absorbance in each solution was determined as described previously (53) using the PeakFit software package (Systat Software, San Jose, CA) and averaged. The SD for the measured maximal absorption wavelength was $\leq$0.4 nm for all dyes in all of the solutions. The behavior of the probes (4-nitrophenol and Reichardt's carboxylated betaine dye) in several solvents (water, n-hexane, and methanol) was tested in the presence and absence of HCl (for 4-nitrophenol) and NaOH (for the betaine dye) at different concentrations of the probes, acid or base. The maximal shifts of the probes were compared to reference values found in the literature. All were within the experimental errors (data not shown). The results of the solvatochromic studies were used to calculate π^*, β, and α as described by Marcus (54).

Determination of the solvent dipolarity/polarizability π^*

The π^* values were determined from the wavenumber (ν_1) of the longest-wavelength Vis absorption band of 4-nitroanisole using the following relationship (54):

$$\pi^* = 0.427(34.12 - \nu_1). \quad (1)$$

Determination of the solvent HBA basicity β

The β values were determined from the wavenumber (ν_2) of the longest-wavelength Vis absorption band of 4-nitrophenol using the following relationship (54):

$$\beta = 0.346(35.045 - \nu_2) - 0.57 \times \pi^*. \quad (2)$$

Determination of the solvent HBD acidity α

The α-values were determined from the longest-wavelength visible absorption band of the 4-[2,6-diphenyl-4-(pyridine-4-yl) pyridinium-1-yl]-2,6-bis(pyridine-3-yl)phenolate (Reichardt's $E_T(8)$ betaine dye) using the relationships in Eqs. 3, 4, and 5:

$$E_T(8)/\left(\text{kcal.mol}^{-1}\right) = 28,591/\lambda_{max}(\text{nm}), \quad (3)$$

where λ_{max} is the wavelength of the maximum of the long-wavelength solvatochromic absorption band of the betaine dye.

The empirical Reichardt's solvent polarity index, $E_T(30)$, was then calculated from the $E_T(8)$ values with the following linear relationship for HBD solvents (55):

$$E_T(30) = [E_T(8) - 16.236]/0.704. \quad (4)$$

Finally, the α-values were calculated from the $E_T(30)$ values according to (54):

$$\alpha = 0.0649 \times E_T(30) - 2.03 - 0.72 \times \pi^*. \quad (5)$$

It has been previously shown (56) that the solvatochromic features of water in aqueous solutions containing small organic compounds and polymers are linearly interrelated as

$$\pi_*^{ij} = z_{io} + a_{io}\alpha_{ij} + \beta_{ij}, \quad (6)$$

where subscript j denotes the concentration of the i-th compound in water; z_{io}, a_{io}, and b_{io} are constants specific for the i-th compound under study.

The interrelationship between z_{io}, a_{io}, and b_{io} for the proteins in this study can be described by

$$b_{io} = 1.81_{0.01} - 1.68_{0.01}z_{io} - 2.07_{0.04}a_{io}. \quad (7)$$

Inclusion of z_{io}-, a_{io}-, and b_{io}-values of PEGs (PEG-1000, PEG-8000, and PEG-10,000) (38) results in a very similar relationship:

$$b_{io} = 1.84_{0.005} - 1.68_{0.005}z_{io} - 2.09_{0.02}a_{io}. \quad (8)$$

The distance of protein i from the reference protein o in terms of z_{io}, a_{io}, and b_{io} may be described as

$$d_{io} = \left\{[(z_{io} - z_o)/z_o]^2 + [(a_{io} - a_o)/a_o]^2 + [(b_{io} - b_o)/b_o]^2\right\}^{0.5}, \quad (9)$$

where d_{io} is the distance of the signature of a given protein i from that of the reference protein o; z_{io}, a_{io}, and b_{io} are the coefficients for the protein i in Eq. 6; and z_o, a_o, and b_o are the coefficients of the reference protein. The dehydrin K_2 was selected as the reference protein o.

Analysis of the data in Table S1 for the different PEGs and dehydrins reveals the relationship between the hydrodynamic radius (R_h) and distance d_{io} as

$$(PD_{50})_i = 1621_{77} - 1165_{62}\log(R_h)_i + 39_{4.9}d_{io}, \quad (10)$$

which is described in more detail in the Results.

Partitioning of K_2 dehydrin and solvatochromic dyes in the aqueous Ficoll-70/PEG-8000 two-phase system

Ficoll-70 (lot 128K1136), with a weight-average molecular weight (M_w) ≅ 70,000, and PEG-8000 (Lot 091M01372V), with a number-average molecular weight (M_n) of 8000, were purchased from Sigma.

Stock solutions of Ficoll-70 (50% w/w) and PEG 8000 (50% w/w) were prepared in deionized water. Stock sodium phosphate buffer (0.5 M (pH 7.4)) was prepared by mixing the appropriate amounts of NaH_2PO_4 and Na_2HPO_4. A mixture of polymers was prepared by dispensing appropriate amounts of the aqueous stock polymer solutions into a 1.2 mL microtube using a Hamilton (Reno, NV) ML-4000 four-probe liquid-handling workstation. Appropriate amounts of stock buffer solutions and water were added to give the ionic and polymer composition required for the final system (after the sample addition—see below) with a total weight of 0.5 g (a total volume of 462 ± 1 μL). All of the aqueous two-phase systems used had the same polymer composition of 19.0% (w/w) Ficoll-70 and 9.0% (w/w) PEG-8000 and the same ionic composition of 0.01 M sodium phosphate buffer (pH 7.4).

An automated instrument for performing aqueous two-phase partitioning, the Automated Signature Workstation (Analiza, Cleveland, OH), was used for the partitioning experiments. The Automated Signature Workstation system is based on the ML-4000 liquid-handling workstation (Hamilton) integrated with a FL600 fluorescence microplate reader (Bio-Tek Instruments, Winooski, VT) and a UV-Vis microplate spectrophotometer (SpectraMax Plus 384; Molecular Devices).

The K_2 dehydrin solution was prepared in water at concentration of 5 mg/mL. Solutions of 4-nitrophenol and 4-nitroanisole at concentrations of 10 and 3 mM, respectively, and a solution of carboxylated Reichardt's betaine dye at a concentration of 4.2 mM were prepared in water. These solutions and their mixtures with dehydrin were prepared in a 1:3 ratio (for 4-nitroanisole) and 1:1 ratio (for the two other dyes); all ratios are by volume.

Varied amounts (0, 20, 40, 60, 80, and 100 μL) of these individual dye solutions, dehydrin solution, or dehydrin-dye mixtures and the corresponding amounts (100, 80, 60, 40, 20, and 0 μL) of water were added to a set of the same polymers/buffer mixtures. The systems were then vortexed in a Multipulse vortexer and centrifuged (Jouan, BR4i; Thermo Fisher Scientific, Waltham, MA) for 60 min at 3500 × *g* at 23°C to accelerate phase settling. The top phase in each system was removed, the interface was discarded, and aliquots from the top and bottom phases were withdrawn in duplicate for analysis using the *o*-phthaldialdehyde (OPA) protein concentration assay or the UV-vis assay.

For the dehydrin partitioning analysis in the absence and presence of dye, 30 μL aliquots from both phases were transferred and diluted with water up to 70 μL and placed into microplate wells. Next, the microplate was sealed and briefly centrifuged (2 min at 1500 rotations per minute). After moderate shaking for 45 min in an incubator at 37°C, 250 μL of OPA reagent was added. After moderate shaking for 4 min at room temperature, the fluorescence was determined using a fluorescence plate reader with a 360 nm excitation filter and a 460 nm emission filter with a sensitivity setting of 100–125.

For the dye partitioning analysis in the absence and presence of dehydrin, 50–120 μL aliquots from both phases were diluted up to 600 μL in 1.2 mL microtubes. Water was used as diluent except for the 4-nitrophenol sample, for which a 20 mM universal buffer (0.01 M each of phosphoric, boric, and acetic acid, adjusted to pH 12.4 with NaOH) was used. After vortexing and a short centrifugation (12 min), aliquots of 250–300 μL were transferred into microplate wells, and the UV-Vis plate reader was used to measure optical absorbance at wavelengths corresponding to the maximal absorption of the dye. The maximal absorption wavelength for each compound was determined in separate experiments by analysis of the absorption spectra over the 240–500 nm range. The concentration of the carboxylated Reichardt's betaine dye, 4-nitrophenol, and 4-nitroanisole in the top and bottom phases of aqueous Ficoll-70/PEG-8000/0.01 M sodium phosphate buffer (pH 7.4) two-phase system was determined by measuring their absorbance at 308, 404, and 318 nm, respectively. In the case of 4-nitrophenol, the maximal absorption was found to be more concentration sensitive in the presence of the universal buffer at pH 12.4. The slope of the linear curve represents the partition coefficient of the dyes in this two-phase system.

In all measurements, the same dilution factor was used for the upper and lower phases, and diluted pure phases were used as blank solutions. The partition coefficient, *K*, is defined as the ratio of the sample concentration in the top phase to that in the bottom phase. The *K*-value for each solute was determined as the slope of the concentration (fluorescence intensity or absorbance, depending on the compound) in the top phase plotted as a function of the concentration in the bottom phase, averaged over the results obtained from two to four partition experiments.

Evaluation of intrinsic disorder propensity of K_2, K_4, and K_{10} dehydrins

The intrinsic disorder propensities of the K_2, K_4, and K_{10} dehydrins were evaluated by a set of commonly used per-residue disorder predictors. This includes PONDR VLXT (57), which is known to have high sensitivity to local sequence peculiarities and can be used for identifying disorder-based interaction sites; PONDR VL3 (58), which is characterized by high accuracy for predicting long intrinsically disordered regions; PONDR VSL2 (59,60), which is one of the more accurate stand-alone disorder predictors (61,62); and a meta predictor PONDR FIT (63) that combines outputs of six predictors of intrinsic disorder (PONDR VLXT (57), PONDR VSL2 (59,60), PONDR VL3 (58), FoldIndex (64), IUPred (65), and TopIDP (66)), making it moderately more accurate than each of its component predictors (63). We also used the IUPred computational platform, which allows identification of either short or long regions of intrinsic disorder (65). The corresponding amino acid sequences and molecular masses of the dehydrins and control proteins are provided in Fig. S1. The outputs of the evaluation of the per-residue disorder propensity by these tools are represented as the real numbers between 1 (ideal prediction of disorder) and 0 (ideal prediction of order). A threshold of ≥0.5 was used to identify disordered residues and regions in query proteins. For each protein, after obtaining an average disorder score from each predictor, all predictor-specific average scores were averaged again to generate an average per-residue intrinsic disorder score. Using a consensus evaluation of intrinsic disorder is motivated by the empirical observations that this approach usually increases the predictive performance compared to the use of just a single predictor (67,68).

RESULTS

Because all the solvatochromic dyes are aromatic compounds prone to binding to proteins, it was necessary to first explore if any of the dyes bind to K_2 dehydrin. The partitioning method in an aqueous two-phase system was used for this purpose as described previously (49). The partition behavior of a protein is very sensitive to the binding of any ligand (69–71); therefore, partitioning of K_2 in the Ficoll-70/PEG-8000/0.01 M sodium phosphate buffer (pH 7.4) was examined in the absence and presence of 4-nitrophenol and 4-nitroanisole using the OPA fluorescence assay. The data presented graphically in Fig. S2 indicate that the partition behavior of dehydrin does not change in the presence of any of the dyes tested ($K_{K2} = 0.299 \pm 0.001$), showing that K_2 does not bind the dyes. The partitioning of dehydrin in the presence of the Reichardt's $E_T(8)$ betaine dye in the two-phase system could not be quantified because of its interference with the OPA assay.

We subsequently examined the partitioning of each of the three dyes in the same two-phase system in the absence and in the presence of the K_2 dehydrin using the UV-vis absorbance assay. Typical data obtained are illustrated in Fig. S3, *A–C* for Reichardt's $E_T(8)$ betaine dye, 4-nitrophenol, and 4-nitroanisole, respectively. The partition coefficients of all three dyes (4-nitrophenol ($K = 1.053 \pm 0.002$), 4-nitroanisole ($K = 1.097 \pm 0.002$), and Reichardt's $E_T(8)$ betaine dye ($K = 2.276 \pm 0.005$)) did not change in the presence of K_2. These data confirm the conclusion that the dyes do not bind to the protein and hence may be used as the molecular probes of the solvent features of aqueous media in the presence of dehydrins.

The solvent features of aqueous media for solutions of K_2, K_4, and K_{10} at different protein concentrations in water were measured (Table 1). The concentration-dependent effect of the protein on the various parameters were extrapolated to higher amounts of dehydrin to facilitate comparison to PEG.

The plots of dipolarity/polarizability (π^*, Fig. 1), HBD acidity (α, Fig. 2), and HBA basicity (β, Fig. 3) show several different patterns for the dehydrins and the nondehydrin control protein HSPB6. In Fig. 1, we see that the K_2 and K_4 dehydrins and HSPB6 have essentially identical effects on π^*, whereas K_{10} has a more pronounced impact on this solvent property. A similar lack of effect on π^* was seen for PEG (38). With HBD α acidity (Fig. 2), HSPB6 induces large changes in α, whereas for dehydrins, there are smaller changes in α that correlate with their length. Lastly, for HBA β basicity (Fig. 3), we see that all compounds have an effect on β with increasing protein concentration. With the dehydrins, the effects can be arranged in the following sequence: $K_{10} > K_4 > K_2$, in which K_2 has only a weak effect. The effect of HSPB6 on β is intermediate between K_4 and K_{10}. The effect appears to be related to the length of the polypeptide chain of a given protein. Analysis of the solvent features of water in aqueous solutions for the dehydrins examined here and the previously examined HSPB6 (39) and ELP (51) show that the relationship described by Eq. 6 holds for all the proteins examined so far. The values of the coefficients determined here and in previous studies are listed in Table 2 with their corresponding statistical characteristics. The likely reason for the relationship described by Eq. 6 seems to be the known cooperativity between the different types of water-water interactions (72).

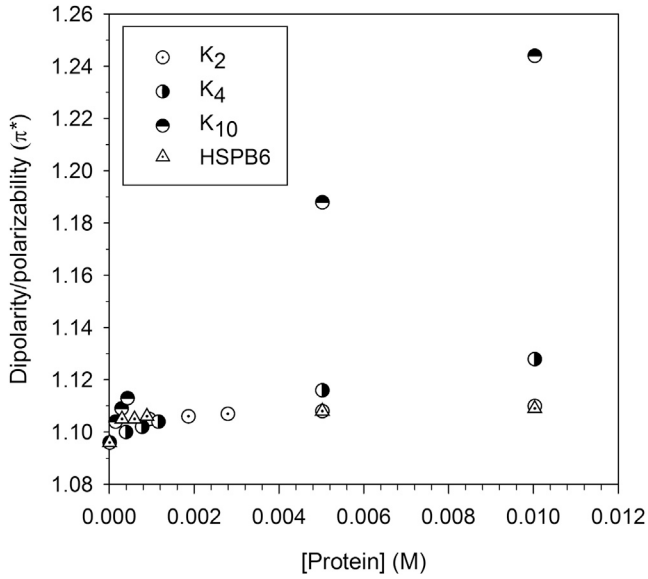

FIGURE 1 Dipolarity/polarizability, π^*, of water in aqueous solution as a function of concentrations of dehydrins K_2, K_4, and K_{10} and the control protein HSPB6. The parameter π^* was calculated using Eq. 1. K_2, dotted circle; K_4, right semifilled circle; K_{10}, top semifilled circle; HSPB6, dotted triangle.

Analysis of the values of coefficients z_o, a_o, and b_o in Table 2 shows that they are interrelated. This interrelationship, shown in Fig. 4, may be described by Eq. 7 ($n = 5$; $r^2 = 0.99998$; SD = 0.012; F = 67,104, where n is the number of proteins (three dehydrins analyzed in this study, HSPB6 (39), and ELP (51)); r^2 is the correlation coefficient; SD is the standard deviation; and F is the ratio of variance).

It should be mentioned that the inclusion of z_{io}-, a_{io}-, and b_{io}-values of PEGs (PEG-1000, PEG-8000, and PEG-10,000) (38) does not change the relationship, as seen in

TABLE 1 Solvent Features of Water in Aqueous Solutions of the K_2, K_4, and K_{10} Dehydrins

Protein	Concentration (mg/mL)	Concentration (mM)	π^*	α	B
No protein	0	0	1.096 (0.002)	1.237 (0.003)	0.596 (0.002)
K_2	5.0	0.93	1.105 (0.001)	1.223 (0.001)	0.597 (0.001)
	10.0	1.86	1.106 (0.001)	1.219 (0.001)	0.599 (0.001)
	15.0	2.79	1.107 (0.001)	1.210 (0.001)	0.600 (0.002)
K_4	5.0	0.38	1.100 (0.001)	1.216 (0.002)	0.597 (0.001)
	10.0	0.76	1.102 (0.001)	1.226 (0.001)	0.599 (0.001)
	15.0	1.14	1.104 (0.001)	1.221 (0.001)	0.600 (0.002)
K_{10}	5.0	0.14	1.104 (0.001)	1.224 (0.002)	0.595 (0.003)
	10.0	0.28	1.109 (0.001)	1.216 (0.001)	0.600 (0.002)
	15.0	0.42	1.113 (0.002)	1.207 (0.002)	0.604 (0.002)

Values in brackets are the SDs.

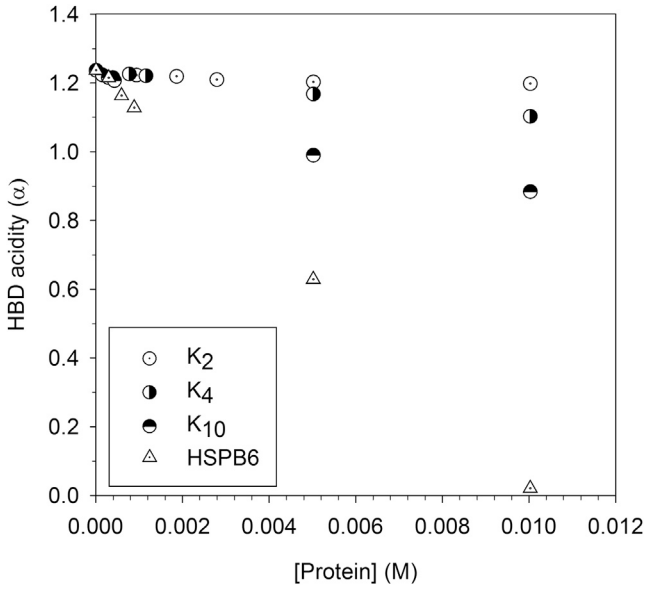

FIGURE 2 HBD acidity, α, of water in aqueous solution as a function of the concentration of dehydrins K_2, K_4, and K_{10} and the control protein HSPB6. The parameter α was calculated using Eqs. 3, 4, and 5. K_2, dotted circle; K_4, right semifilled circle; K_{10}, top semifilled circle; HSPB6, dotted triangle.

Eq. 8 ($n = 8$; $r^2 = 0.99998$; SD = 0.010; F = 114,316, where all parameters are as previously defined).

The specific coefficients of Eq. 6 describe the relationships between the solvent features of water in the aqueous solutions of the proteins examined in this study and the previously studied HSPB6 and ELP. Hence, the set of coefficients determined for each macromolecule may be viewed as a signature of its effect on the solvent features of water.

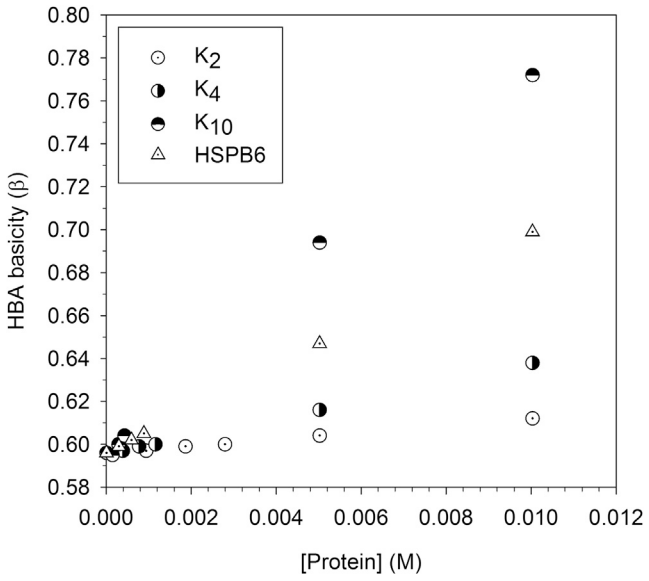

FIGURE 3 HBA basicity, β, of water in aqueous solution as a function of the concentration of dehydrins K_2, K_4, and K_{10} and the control protein HSPB6. The parameter β was calculated using Eq. 2. K_2, dotted circle; K_4, right semifilled circle; K_{10}, top semifilled circle; HSPB6, dotted triangle.

TABLE 2 Coefficients z_o, a_o, and b_o for the Proteins Indicated and Their Euclidean Distance d_{io} from the K_2 Dehydrin

Protein	Coefficient z_o	Coefficient a_o	Coefficient b_o	Distance d_{io}
K_2	0.96 (0.03)	−0.066 (0.007)	0.37 (0.04)	0
K_4	0.32 (0.02)	−0.116 (0.007)	1.55 (0.03)	3.35
K_{10}	2.23(0.09)	−0.69 (0.03)	−0.46 (0.098)	9.81
HSP6B	−2.34 (1.60)	0.32 (0.18)	5.1 (2.3)	14.47
ELP	1.87 (0.04)	−0.54 (0.03)	−0.19 (0.05)	7.40

Values in brackets are the SDs. Coefficients z_o, a_o, and b_o are calculated from Eq. 6, with their Euclidean distance d_{io} from Eq. 9.

Note that the use of 1 M NaOH and 1 M HCl is necessary to ensure that there is sufficient signal intensity from the carboxylated Reichardt's betaine dye and the 4-nitrophenol (73). Therefore, buffers with a specific pH cannot be used. Because all of the proteins used in this study are IDPs, we do not expect structural changes due to pH to be an issue. Also, the lack of difference between in the relationship in Eq. 7 (proteins only) and Eq. 8 (proteins and nonionic PEG) suggests that the changes in pH have not altered the proteins' solvent properties, providing indirect evidence of a lack of change in their structure.

To compare the effects of the different proteins on water, we can estimate the distances for different proteins from a protein chosen as the reference. Here, the distance of protein i from the reference protein o may be described as shown in Eq. 9, in which the dehydrin K_2 was selected as the reference protein o. The distances, d_{io}, between the proteins and polymers examined and dehydrin K_2, are presented in Table S1 together with their corresponding R_h and PD_{50}

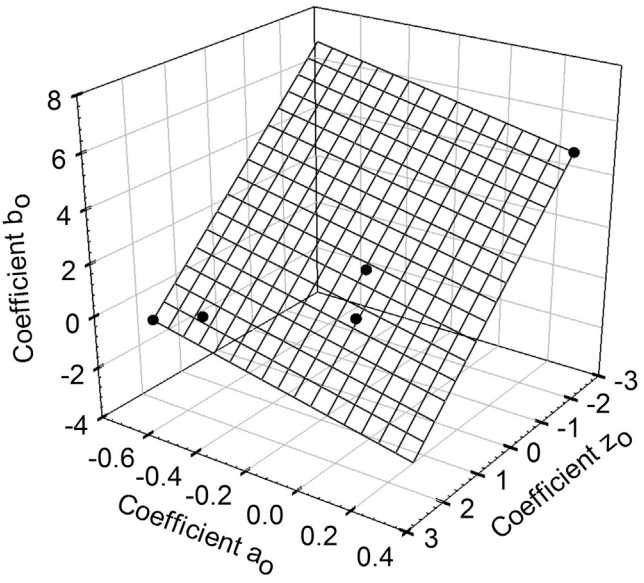

FIGURE 4 Interrelationship between coefficients z_o, a_o, and b_o characterizing solvent features of water in the presence of dehydrins K_2, K_4, and K_{10} and the control proteins HSPB6 and ELP (see Eq. 7).

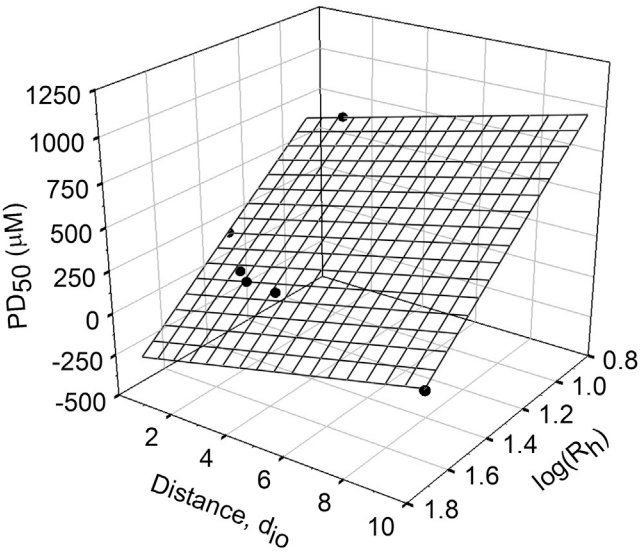

FIGURE 5 The efficiency of LDH cryoprotection (PD_{50}) as a function of the size of the compound ($\log(R_h)$) and the distance (d_{io})(from Eqs. 9 to 10).

values. As noted in the Introduction, PD_{50} values represent the concentration of additive required to recover 50% of LDH activity after multiple freeze/thaw treatments and hence reflect the efficiency of cryoprotection of a given additive. Analysis of the data in Table S1 for the different PEGs and dehydrins reveals the relationship illustrated in Fig. 5 and defined in Eq. 10 ($n = 6$; $r^2 = 0.992$; SD = 28.6; F = 190.5). This suggest that the PD_{50} value of a particular compound can be described as related to the hydrodynamic size of the compound (R_h) and to the compound's effect on solvent properties of water.

DISCUSSION

Many studies (see, for example, (35,36,74–78)) have shown that dehydrins are able to protect LDH enzyme activity from damage caused by freezing and thawing. In our previous work, we suggested that the molecular shield effect (35,36) dominates the dehydrin protection mechanism based on the observation that the cryoprotective effects of PEGs were very similar to the effect of dehydrins (36). Secondly, we found that the effectiveness of the protection (the PD_{50} value) was related to the hydrodynamic dimensions of the additive (the R_h); in essence, the larger the dehydrin or PEG, the more efficient the protection. However, at larger R_h, the PD_{50} relationship becomes asymptotic (cf. Fig. 4 from Hughes et al. (36)). Secondly, not all polar, disordered proteins have a protective effect in the LDH assay. Frost—an intrinsically disordered, cold-response protein in *Drosophila*—is a protein rich in Pro, Glu, Ser, and Thr. It was found to have a protective effect worse than negative control proteins such as lysozyme despite Frost's large R_h (79). If the cryoprotective effect was solely driven by a molecular shield effect originating from hard, steric interactions, one would expect that the larger dehydrins and PEG molecules would always be more efficient than the smaller ones.

Therefore, the effect of dehydrins or PEG are significantly more complex than just excluded volume (or molecular shield) mechanisms. Although the increase in the concentration of crowding agent (dehydrins or PEG, in our case) would decrease volume accessible to LDH, the concentration of an aggregating protein (LDH) in the available volume (i.e., the volume free from crowders) will increase, thereby increasing aggregation probability. In fact, for several proteins that can form amyloid-like fibrils, it was shown that the aggregation kinetics can be dramatically accelerated in a crowded environment (80–86). Furthermore, the efficiency of excluded volume effects posed by a crowder is known to be dependent on the relative hydrodynamic dimensions of crowder and target molecule ("crowdee"), with the strongest effects being ascribed to a situation when crowder and crowdee have comparable hydrodynamic volumes (87–90). However, when the crowder volume becomes too large, larger "caves" will be formed between the crowder molecules that could accumulate more than one molecule of crowdee. In other words, although the globally accessible volume will decrease, the locally accessible volume might increase (87).

Importantly, the observed differences in cryoprotective properties of dehydrins cannot be attributed to the variability of their overall degree of disorder. As it follows from Fig. 6, all three dehydrins analyzed in our study were characterized by disorder profiles typical for the mostly disordered proteins, possessing high mean disorder scores of 0.91 ± 0.05, 0.90 ± 0.05, and 0.90 ± 0.05 for K_2, K_4, and K_{10}, respectively. Such very close similarity of the mean disorder scores of these three dehydrins is rather unexpected. In fact, although the K_4 and K_{10} dehydrins are concatemers of the K_2 protein (36) and although the sequence of the K_2 dehydrin constitutes an integral part of the K_4 and K_{10} dehydrins, the K_4 and K_{10} dehydrins contain an additional one (K_4) or four (K_{10}) 20-residue-long linker segment connecting the repeating K_2 sequences.

Our results show that the effect of dehydrins on solvent properties of water represents one of the possible contributors to the cryoprotective properties of these proteins. Fig. 5 shows that there is a relationship between the PD_{50} value, the logarithm of R_h, and a combination of the three solvent properties of water examined (dipolarity/polarizability, HBD acidity, and HBA basicity). The results can be interpreted assuming that the R_h (i.e., the hydrodynamic volume) of the compound has an effect on the PD_{50} value (negative correlation, recalling that smaller PD_{50} values mean higher cryoprotective efficiency), but as the R_h increases, this increased efficiency becomes limited by the stronger effects of the larger dehydrins on the solvent properties of water (π^*, α, and β).

The use of dehydrins and several PEGs of different sizes (PEG-1000, PEG-8000, and PEG-10,000) provides an opportunity to further compare PD_{50}, R_h, and solvent effects.

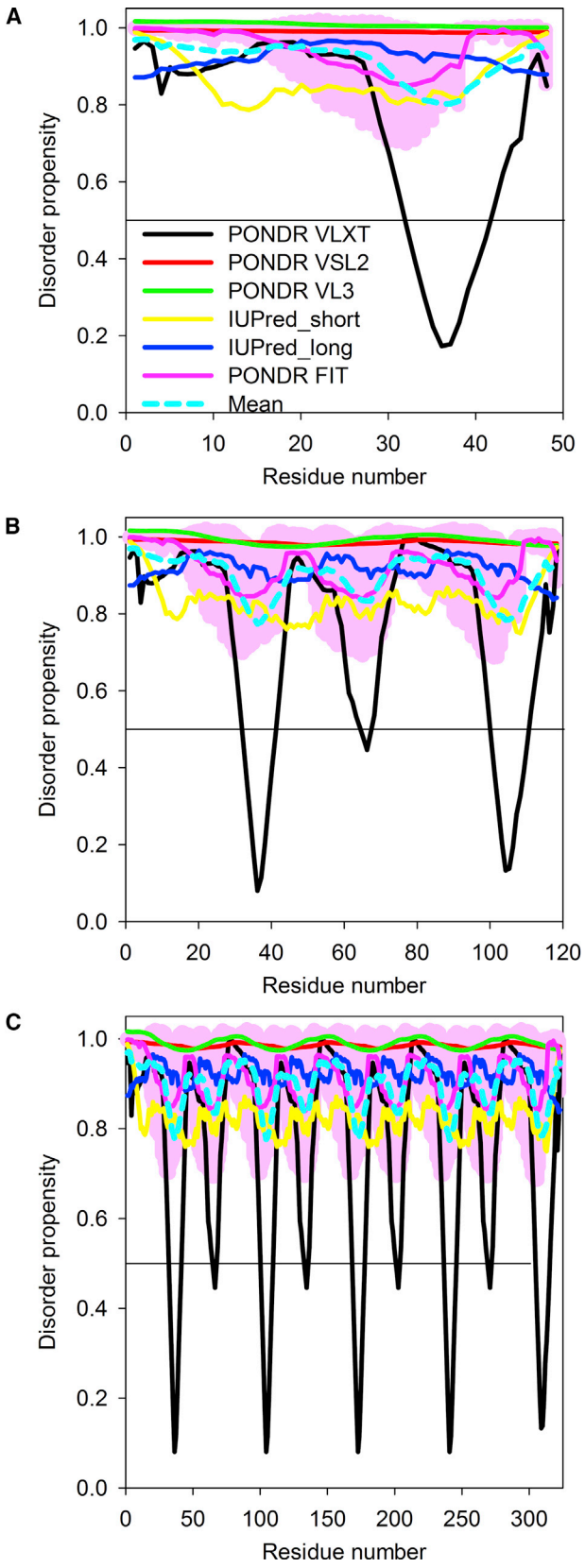

FIGURE 6 Evaluation of intrinsic disorder propensity of (*A*) K_2, (*B*) K_4, and (*C*) K_{10} dehydrins. Disorder profiles representing per-residue disorder predispositions of these proteins were generated by PONDR VLXT, PONDR VSL2, PONDR VL3, PONDR FIT, IUPred_short, and IUPred_long, with the corresponding results shown by black, red, green, pink, yellow, and blue lines, respectively. Dashed cyan lines show the mean disorder propensity calculated for each protein by averaging disorder profiles of individual predictors. The light pink shadow around the PONDR FIT shows error distribution. In these analyses, the predicted intrinsic disorder scores above 0.5 are considered to correspond to the disordered residues/regions, whereas regions with the disorder scores between 0.2 and 0.5 are considered flexible. To see this figure in color, go online.

The most notable differences are that in all cases (Fig. 1, 2, and 3), K_{10} had the strongest effect on the solvent properties, whereas K_2 had very little effect on them and K_4 had little effect on dipolarity/polarizability (π^*) and HBD acidity (α). All proteins had a relatively large effect on HBA basicity (β). These observations may explain the established difference in the cryoprotective efficiency of dehydrins, in which for the larger dehydrins (i.e., the larger R_h), other effects on the solvent properties (as reflected in π^*, α, and β) may "override" the volume exclusion effect. The dramatic difference in HBA β leads us to speculate that dehydrins affect the ability of hydrogen bonding in bulk water, which may also have an effect on how the proteins form hydrogen bonds as well. It is important to note here that the largest PEG used, PEG-10,000, has an identical PD_{50} to PEG-8000 despite the difference in R_h. It is also interesting to note that PEGs were unable to recover 100% LDH activity, whereas dehydrins usually do, suggesting that there could be some solvent effect differences between the two compounds that have yet to be identified.

CONCLUSIONS

The results presented here show that the limiting efficiency of larger cryoprotective agents may come from the effect of these agents on the solvent properties of bulk water. The challenge now is to understand what the physical basis for this limiting effect is, which is well beyond the scope of this work. The effect of dehydrins on solvent properties may also provide part of an answer to the basic question—why are plants using dehydrin proteins rather than some specific secondary metabolites, especially because plants are generally very good at making these? The effect of dehydrins on HBA β suggests that proteins could have better tunable effects on this solvent property of water than a simple, repeating polymer (such as PEG). An additional explanation is that by using proteins, the plants can reuse the amino acids for other needs once the abiotic stress has abated.

SUPPORTING MATERIAL

Three figures and one table are available at http://www.biophysj.org/biophysj/supplemental/S0006-3495(18)31066-X.

AUTHOR CONTRIBUTIONS

B.Z., V.N.U., and S.P.G. designed the study and wrote the manuscript. A.W.M. expressed and purified the dehydrins, and L.A.F. performed the solvatochromic dye assays and partitioning studies. All authors analyzed the results and approved the final version of the manuscript.

ACKNOWLEDGMENTS

This work was supported by a Natural Sciences and Engineering Research Council of Canada Discovery Grant to S.P.G.

REFERENCES

1. Wright, P. E., and H. J. Dyson. 1999. Intrinsically unstructured proteins: re-assessing the protein structure-function paradigm. *J. Mol. Biol.* 293:321–331.
2. Uversky, V. N., J. R. Gillespie, and A. L. Fink. 2000. Why are "natively unfolded" proteins unstructured under physiologic conditions? *Proteins.* 41:415–427.
3. Dunker, A. K., J. D. Lawson, …, Z. Obradovic. 2001. Intrinsically disordered protein. *J. Mol. Graph. Model.* 19:26–59.
4. Uversky, V. N. 2002. Natively unfolded proteins: a point where biology waits for physics. *Protein Sci.* 11:739–756.
5. Tompa, P. 2002. Intrinsically unstructured proteins. *Trends Biochem. Sci.* 27:527–533.
6. Uversky, V. N., and A. K. Dunker. 2010. Understanding protein nonfolding. *Biochim. Biophys. Acta.* 1804:1231–1264.
7. Uversky, V. N., and A. K. Dunker. 2012. Multiparametric analysis of intrinsically disordered proteins: looking at intrinsic disorder through compound eyes. *Anal. Chem.* 84:2096–2104.
8. Uversky, V. N. 2015. Biophysical methods to investigate intrinsically disordered proteins: avoiding an "Elephant and Blind Men" situation. *In* Intrinsically Disordered Proteins Studied by NMR Spectroscopy. Springer, pp. 215–260.
9. Xue, B., R. L. Dunbrack, …, V. N. Uversky. 2010. PONDR-FIT: a meta-predictor of intrinsically disordered amino acids. *Biochim. Biophys. Acta.* 1804:996–1010.
10. Dosztányi, Z. 2018. Prediction of protein disorder based on IUPred. *Protein Sci.* 27:331–340.
11. Dunker, K. A., C. J. Brown, and Z. Obradovic. 2002. Identification and functions of usefully disordered proteins. *In* Unfolded Proteins. Elsevier, pp. 25–49.
12. Iakoucheva, L. M., C. J. Brown, …, A. K. Dunker. 2002. Intrinsic disorder in cell-signaling and cancer-associated proteins. *J. Mol. Biol.* 323:573–584.
13. Uversky, V. N. 2011. Flexible nets of malleable guardians: intrinsically disordered chaperones in neurodegenerative diseases. *Chem. Rev.* 111:1134–1166.
14. Sun, X., E. H. Rikkerink, …, V. N. Uversky. 2013. Multifarious roles of intrinsic disorder in proteins illustrate its broad impact on plant biology. *Plant Cell.* 25:38–55.
15. Close, T. J. 1997. Dehydrins: a commonalty in the response of plants to dehydration and low temperature. *Physiol. Plant.* 100:291–296.
16. Hara, M. 2010. The multifunctionality of dehydrins: an overview. *Plant Signal. Behav.* 5:503–508.
17. Eriksson, S. K., and P. Harryson. 2011. Dehydrins: molecular biology, structure and function. *In* Plant Desiccation Tolerance, *Volume 215*. Springer, pp. 289–305.
18. Allagulova, Ch. R., F. R. Gimalov, …, V. A. Vakhitov. 2003. The plant dehydrins: structure and putative functions. *Biochemistry (Mosc.).* 68:945–951.
19. Graether, S. P., and K. F. Boddington. 2014. Disorder and function: a review of the dehydrin protein family. *Front. Plant Sci.* 5:576.
20. Galau, G. A., D. W. Hughes, and L. Dure, III. 1986. Abscisic acid induction of cloned cotton late embryogenesis-abundant (Lea) mRNAs. *Plant Mol. Biol.* 7:155–170.
21. Battaglia, M., Y. Olvera-Carrillo, …, A. A. Covarrubias. 2008. The enigmatic LEA proteins and other hydrophilins. *Plant Physiol.* 148:6–24.
22. Hincha, D. K., and A. Thalhammer. 2012. LEA proteins: IDPs with versatile functions in cellular dehydration tolerance. *Biochem. Soc. Trans.* 40:1000–1003.
23. Tunnacliffe, A., and M. J. Wise. 2007. The continuing conundrum of the LEA proteins. *Naturwissenschaften.* 94:791–812.
24. Close, T. J. 1996. Dehydrins: emergence of a biochemical role of a family of plant dehydration proteins. *Physiol. Plant.* 97:795–803.
25. Malik, A. A., M. Veltri, …, S. P. Graether. 2017. Genome analysis of conserved dehydrin motifs in vascular plants. *Front. Plant Sci.* 8:709.
26. Hara, M., M. Fujinaga, and T. Kuboi. 2005. Metal binding by citrus dehydrin with histidine-rich domains. *J. Exp. Bot.* 56:2695–2703.
27. Richard Strimbeck, G. 2017. Hiding in plain sight: the F segment and other conserved features of seed plant SKn dehydrins. *Planta.* 245:1061–1066.
28. Liu, C.-C., C.-M. Li, …, C.-P. Yang. 2012. Genome-wide identification and characterization of a dehydrin gene family in poplar (Populus trichocarpa). *Plant Mol. Biol. Report.* 30:848–859.
29. Houde, M., S. Dallaire, …, F. Sarhan. 2004. Overexpression of the acidic dehydrin WCOR410 improves freezing tolerance in transgenic strawberry leaves. *Plant Biotechnol. J.* 2:381–387.
30. Labhilili, M., P. Joudrier, and M.-F. Gautier. 1995. Characterization of cDNAs encoding Triticum durum dehydrins and their expression patterns in cultivars that differ in drought tolerance. *Plant Sci.* 112:219–230.
31. Saibi, W., K. Feki, …, F. Brini. 2015. Durum wheat dehydrin (DHN-5) confers salinity tolerance to transgenic Arabidopsis plants through the regulation of proline metabolism and ROS scavenging system. *Planta.* 242:1187–1194.
32. Rinne, P. L., P. L. Kaikuranta, …, C. van der Schoot. 1999. Dehydrins in cold-acclimated apices of birch (Betula pubescens ehrh.): production, localization and potential role in rescuing enzyme function during dehydration. *Planta.* 209:377–388.
33. Banerjee, A., and A. Roychoudhury. 2015. Group II late embryogenesis abundant (LEA) proteins: structural and functional aspects in plant abiotic stress. *Plant Growth Regul.* 79:1–17.
34. Liu, Y., L. Wang, …, D. Li. 2017. Functional characterization of KS-type dehydrin ZmDHN13 and its related conserved domains under oxidative stress. *Sci. Rep.* 7:7361.
35. Hughes, S., and S. P. Graether. 2011. Cryoprotective mechanism of a small intrinsically disordered dehydrin protein. *Protein Sci.* 20:42–50.
36. Hughes, S. L., V. Schart, …, S. P. Graether. 2013. The importance of size and disorder in the cryoprotective effects of dehydrins. *Plant Physiol.* 163:1376–1386.
37. Tompa, P., P. Bánki, …, K. Tompa. 2006. Protein-water and protein-buffer interactions in the aqueous solution of an intrinsically unstructured plant dehydrin: NMR intensity and DSC aspects. *Biophys. J.* 91:2243–2249.
38. Ferreira, L. A., V. N. Uversky, and B. Y. Zaslavsky. 2017. Role of solvent properties of water in crowding effects induced by macromolecular agents and osmolytes. *Mol. Biosyst.* 13:2551–2563.
39. Ferreira, L. A., V. N. Uversky, and B. Y. Zaslavsky. 2018. Phase equilibria, solvent properties, and protein partitioning in aqueous polyethylene glycol-600-trimethylamine N-oxide and polyethylene glycol-600-choline chloride two-phase systems. *J. Chromatogr. A.* 1535:154–161.
40. Ferreira, L. A., V. N. Uversky, and B. Y. Zaslavsky. 2017. Effects of the Hofmeister series of sodium salts on the solvent properties of water. *Phys. Chem. Chem. Phys.* 19:5254–5261.

41. Taft, R. W., and M. J. Kamlet. 1976. The solvatochromic comparison method. 2. The alpha-scale of solvent hydrogen-bond donor (HBD) acidities. *J. Am. Chem. Soc.* 98:2886–2894.

42. Kamlet, M. J., and R. W. Taft. 1976. The solvatochromic comparison method. 1. The beta-scale of solvent hydrogen-bond acceptor (HBA) basicities. *J. Am. Chem. Soc.* 98:377–383.

43. Kamlet, M. J., J. L. Abboud, and R. W. Taft. 1976. The solvatochromic comparison method. 6. The pi* scale of solvent polarities. *J. Am. Chem. Soc.* 99:6027–6038.

44. Vitha, M., and P. W. Carr. 2006. The chemical interpretation and practice of linear solvation energy relationships in chromatography. *J. Chromatogr. A.* 1126:143–194.

45. Kamlet, M. J., R. M. Doherty, …, R. W. Taft. 1988. Linear solvation energy relationships. 44. Parameter estimation rules that allow accurate prediction of octanol/water partition coefficients and other solubility and toxicity properties of polychlorinated biphenyls and polycyclic aromatic hydrocarbons. *Environ. Sci. Technol.* 22:503–509.

46. Kamlet, M. J., R. M. Doherty, …, R. W. Taft. 1987. Solubility properties in biological media 9: prediction of solubility and partition of organic nonelectrolytes in blood and tissues from solvatochromic parameters. *J. Pharm. Sci.* 76:14–17.

47. Carr, P. W., R. M. Doherty, …, C. Horvath. 1986. Study of temperature and mobile-phase effects in reversed-phase high-performance liquid chromatography by the use of the solvatochromic comparison method. *Anal. Chem.* 58:2674–2680.

48. Ab Rani, M. A., A. Brant, …, R. Wilding. 2011. Understanding the polarity of ionic liquids. *Phys. Chem. Chem. Phys.* 13:16831–16840.

49. Ferreira, L. A., P. P. Madeira, …, B. Y. Zaslavsky. 2016. Role of solvent properties of aqueous media in macromolecular crowding effects. *J. Biomol. Struct. Dyn.* 34:92–103.

50. Ferreira, L. A., L. Breydo, …, B. Y. Zaslavsky. 2017. Effects of osmolytes on solvent features of water in aqueous solutions. *J. Biomol. Struct. Dyn.* 35:1055–1068.

51. Ferreira, L. A., J. T. Cole, …, B. Y. Zaslavsky. 2015. Solvent properties of water in aqueous solutions of Elastin-like polypeptide. *Int. J. Mol. Sci.* 16:13528–13547.

52. Reichardt, C., E. H. Görnert, and G. Schäfer. 1988. Über Pyridinium-N-phenolat-Betaine und ihre Verwendung zur Charakterisierung der Polarität von Lösungsmitteln, XI. Herstellung und UV/VIS-spektroskopische Eigenschaften eines wasserlöslichen Carboxylat-substituierten Pyridinium-N-phenolat-Betainfarbstoffs. *Eur. J. Org. Chem.* 1988:839–844.

53. Huddleston, J. G., H. D. Willauer, and R. D. Rogers. 2002. The solvatochromic properties, α, β, and π*, of PEG-salt aqueous biphasic systems. *Phys. Chem. Chem. Phys.* 4:4065–4070.

54. Marcus, Y. 1993. The properties of organic liquids that are relevant to their use as solvating solvents. *Chem. Soc. Rev.* 22:409–416.

55. Reichardt, C., D. Che, …, G. Schäfer. 2001. Syntheses and UV/Vis-spectroscopic properties of hydrophilic 2-, 3-, and 4-pyridyl-substituted solvatochromic and halochromic pyridinium N-phenolate betaine dyes as new empirical solvent polarity indicators. *Eur. J. Org. Chem.* 2001:2343–2361.

56. Ferreira, L. A., J. A. Loureiro, …, B. Y. Zaslavsky. 2016. Why physicochemical properties of aqueous solutions of various compounds are linearly interrelated. *J. Mol. Liq.* 221:116–123.

57. Romero, P., Z. Obradovic, …, A. K. Dunker. 2001. Sequence complexity of disordered protein. *Proteins.* 42:38–48.

58. Obradovic, Z., K. Peng, …, A. K. Dunker. 2003. Predicting intrinsic disorder from amino acid sequence. *Proteins.* 53 (*Suppl 6*):566–572.

59. Obradovic, Z., K. Peng, …, A. K. Dunker. 2005. Exploiting heterogeneous sequence properties improves prediction of protein disorder. *Proteins.* 61 (*Suppl 7*):176–182.

60. Peng, K., S. Vucetic, …, Z. Obradovic. 2005. Optimizing long intrinsic disorder predictors with protein evolutionary information. *J. Bioinform. Comput. Biol.* 3:35–60.

61. Peng, Z. L., and L. Kurgan. 2012. Comprehensive comparative assessment of in-silico predictors of disordered regions. *Curr. Protein Pept. Sci.* 13:6–18.

62. Fan, X., and L. Kurgan. 2014. Accurate prediction of disorder in protein chains with a comprehensive and empirically designed consensus. *J. Biomol. Struct. Dyn.* 32:448–464.

63. Xue, B., R. W. Williams, …, V. N. Uversky. 2010. Archaic chaos: intrinsically disordered proteins in Archaea. *BMC Syst. Biol.* 4 (*Suppl 1*):S1.

64. Prilusky, J., C. E. Felder, …, J. L. Sussman. 2005. FoldIndex: a simple tool to predict whether a given protein sequence is intrinsically unfolded. *Bioinformatics.* 21:3435–3438.

65. Dosztányi, Z., V. Csizmók, …, I. Simon. 2005. IUPred: web server for the prediction of intrinsically unstructured regions of proteins based on estimated energy content. *Bioinformatics.* 21:3433–3434.

66. Campen, A., R. M. Williams, …, A. K. Dunker. 2008. TOP-IDP-scale: a new amino acid scale measuring propensity for intrinsic disorder. *Protein Pept. Lett.* 15:956–963.

67. Walsh, I., M. Giollo, …, S. C. Tosatto. 2015. Comprehensive large-scale assessment of intrinsic protein disorder. *Bioinformatics.* 31:201–208.

68. Peng, Z., and L. Kurgan. 2011. On the complementarity of the consensus-based disorder prediction. *Pac. Symp. Biocomput.* 2012:176–187.

69. Zaslavsky, A., N. Gulyaeva, …, B. Zaslavsky. 2001. A new method for analysis of components in a mixture without preseparation: evaluation of the concentration ratio and protein-protein interaction. *Anal. Biochem.* 296:262–269.

70. Fedotoff, O., L. M. Mikheeva, …, B. Y. Zaslavsky. 2012. Influence of serum proteins on conformation of prostate-specific antigen. *J. Biomol. Struct. Dyn.* 29:1051–1064.

71. Backman, L. 2000. Detection and analysis of interactions by two-phase partition. *In* Aqueous Two-Phase Systems: Methods and Protocols. R. Hatti-Kaul, ed. Humana Press, pp. 219–228.

72. Madeira, P. P., A. Bessa, …, B. Y. Zaslavsky. 2015. Cooperativity between various types of polar solute-solvent interactions in aqueous media. *J. Chromatogr. A.* 1408:108–117.

73. Ferreira, L. A., N. B. Gusev, …, B. Y. Zaslavsky. 2018. Effect of human heat shock protein HspB6 on the solvent features of water in aqueous solutions. *J. Biomol. Struct. Dyn.* 36:1520–1528.

74. Wisniewski, M., R. Webb, …, M. Griffith. 1999. Purification, immunolocalization, cryoprotective, and antifreeze activity of PCA60: a dehydrin from peach (Prunus persica). *Physiol. Plant.* 105:600–608.

75. Reyes, J. L., F. Campos, …, A. A. Covarrubias. 2008. Functional dissection of hydrophilins during in vitro freeze protection. *Plant Cell Environ.* 31:1781–1790.

76. Hara, M., T. Endo, …, A. Kameyama. 2017. The role of hydrophobic amino acids of K-segments in the cryoprotection of lactate dehydrogenase by dehydrins. *J. Plant Physiol.* 210:18–23.

77. Drira, M., W. Saibi, …, M. Hanin. 2013. The K-segments of the wheat dehydrin DHN-5 are essential for the protection of lactate dehydrogenase and β-glucosidase activities in vitro. *Mol. Biotechnol.* 54:643–650.

78. Hernández-Sánchez, I. E., D. M. Martynowicz, …, J. F. Jiménez-Bremont. 2014. A dehydrin-dehydrin interaction: the case of SK3 from Opuntia streptacantha. *Front. Plant Sci.* 5:520.

79. Newman, C. E., J. Toxopeus, …, A. Percival-Smith. 2017. CRISPR-induced null alleles show that *Frost* protects *Drosophila melanogaster* reproduction after cold exposure. *J. Exp. Biol.* 220:3344–3354.

80. Uversky, V. N., E. M Cooper, …, A. L. Fink. 2002. Accelerated alpha-synuclein fibrillation in crowded milieu. *FEBS Lett.* 515:99–103.

81. Hatters, D. M., A. P. Minton, and G. J. Howlett. 2002. Macromolecular crowding accelerates amyloid formation by human apolipoprotein C-II. *J. Biol. Chem.* 277:7824–7830.

82. Ellis, R. J., and A. P. Minton. 2006. Protein aggregation in crowded environments. *Biol. Chem.* 387:485–497.

83. Munishkina, L. A., A. Ahmad, …, V. N. Uversky. 2008. Guiding protein aggregation with macromolecular crowding. *Biochemistry.* 47:8993–9006.

84. Zhou, Z., J. B. Fan, …, Y. Liang. 2009. Crowded cell-like environment accelerates the nucleation step of amyloidogenic protein misfolding. *J. Biol. Chem.* 284:30148–30158.

85. Ma, B., J. Xie, …, W. Li. 2013. Macromolecular crowding modulates the kinetics and morphology of amyloid self-assembly by β-lactoglobulin. *Int. J. Biol. Macromol.* 53:82–87.

86. Kuznetsova, I. M., K. K. Turoverov, and V. N. Uversky. 2014. What macromolecular crowding can do to a protein. *Int. J. Mol. Sci.* 15:23090–23140.

87. Zhou, H. X. 2008. Effect of mixed macromolecular crowding agents on protein folding. *Proteins.* 72:1109–1113.

88. Batra, J., K. Xu, …, H. X. Zhou. 2009. Effect of macromolecular crowding on protein binding stability: modest stabilization and significant biological consequences. *Biophys. J.* 97:906–911.

89. Christiansen, A., Q. Wang, …, P. Wittung-Stafshede. 2010. Factors defining effects of macromolecular crowding on protein stability: an in vitro/in silico case study using cytochrome c. *Biochemistry.* 49:6519–6530.

90. Shahid, S., M. I. Hassan, …, F. Ahmad. 2017. Size-dependent studies of macromolecular crowding on the thermodynamic stability, structure and functional activity of proteins: in vitro and in silico approaches. *Biochim. Biophys. Acta, Gen. Subj.* 1861:178–197.

Biophysical Journal, Volume *115*

Supplemental Information

Effect of an Intrinsically Disordered Plant Stress Protein on the Properties of Water

Luisa A. Ferreira, Alicyia Walczyk Mooradally, Boris Zaslavsky, Vladimir N. Uversky, and Steffen P. Graether

Supporting Material

Table S1. PD_{50}, R_h and d_{io} of compounds used in the fit of eqn. 10.

Compound	**PD_{50} (μM)**	**R_h (Å)**	**d_{io}**
K_2	122.3	18.90	0.00
K_4	61.2	30.20	3.35
K_{10}	26.6	49.30	9.81
PEG-1000	662.0	7.48	1.41
PEG-8000	24.0	24.55	1.33
PEG-10,000	33.2	27.88	2.01

Sequence of K_2 (Mr 5381.25)
MKEKIKERIPGMGRKDEQKQTSATSTPGQGQQQKGMMEKIKEKLPGAH

Sequence of K_4 (Mr 13144.04)
MKEKIKERIPGMGRKDEQKQTSATSTPGQGQQQKGMMEKIKEKLPGAHLDRKDEQKQTSATSTP
GQGQMKEKIKERIPGMGRKDEQKQTSATSTPGQGQQQKGMMEKIKEKLPGAHLE

Sequence of K_{10} (Mr 35705.58)
MKEKIKERIPGMGRKDEQKQTSATSTPGQGQQQKGMMEKIKEKLPGAHLDRKDEQKQTSATSTP
GQGQMKEKIKERIPGMGRKDEQKQTSATSTPGQGQQQKGMMEKIKEKLPGAHLDRKDEQKQTSA
TSTPGQGQMKEKIKERIPGMGRKDEQKQTSATSTPGQGQQQKGMMEKIKEKLPGAHLDRKDEQK
QTSATSTPGQGQMKEKIKERIPGMGRKDEQKQTSATSTPGQGQQQKGMMEKIKEKLPGAHLDRK
DEQKQTSATSTPGQGQMKEKIKERIPGMGRKDEQKQTSATSTPGQGQQQKGMMEKIKEKLPGAH
LE

Sequence of HSPB6 (Mr 17135.60)
MEIPVPVQPSWLRRASAPLPGLSAPGRLFDQRFGEGLLEAELAALCPTTLAPYYLRAPSVALPV
AQVPTDPGHFSVLLDVKHFSPEEIAVKVVGEHVEVHARHEERPDEHGFVAREFHRRYRLPPGVD
PAAVTSALSPEGVLSIQAAPASAQAPPPAAAK

Sequence of ELP (Mr 17063.21)
MGH(GVGVP)$_{40}$GWP

Figure S1. Dehydrin and Control Protein Sequences

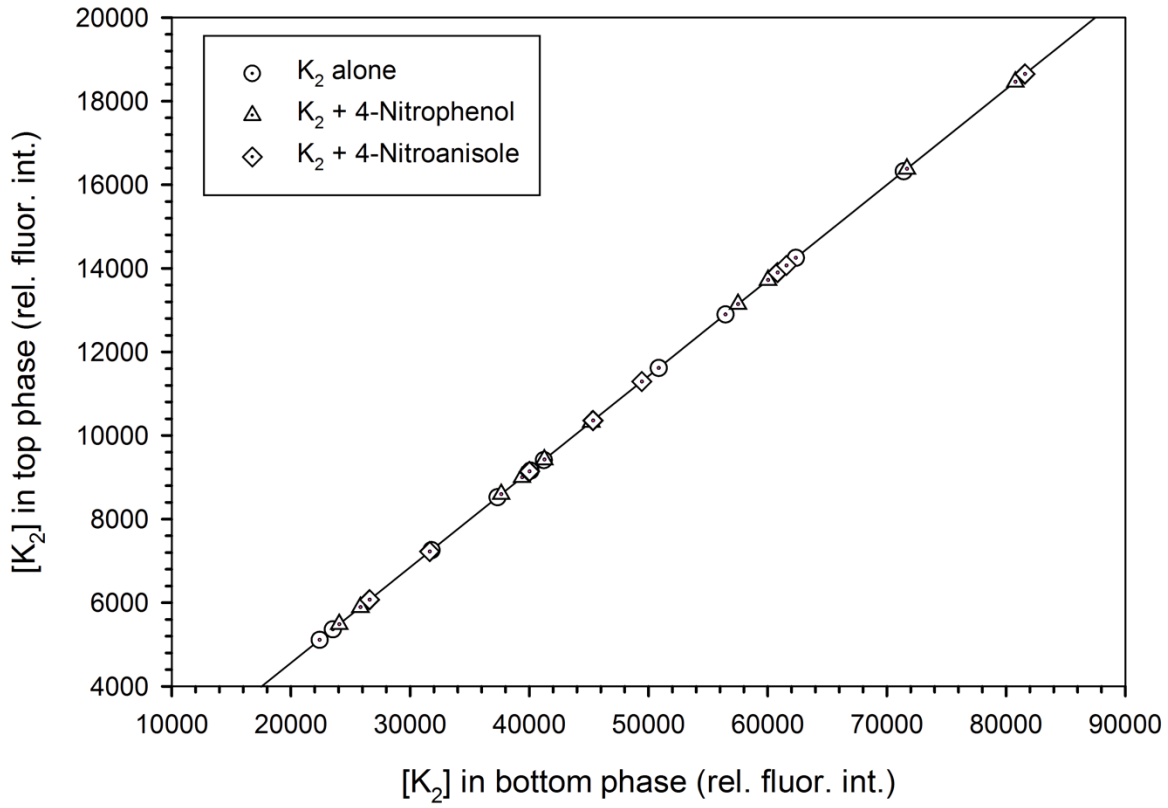

Figure S2. K_2 distribution is unaffected by the presence of the dyes. Partitioning of K_2 dehydrin in the presence and absence of 4-nitrophenol and 4-nitroanisole in the top and bottom phases of aqueous Ficoll-70/PEG-8000/0.01 M sodium phosphate buffer. The slope of the linear curve represents the partition coefficient of the K_2 dehydrin. K_2 alone, dotted circle; K_2 with 4-nitrophenol, dotted triangle; K_2 with 4-nitroanisole, dotted diamond.

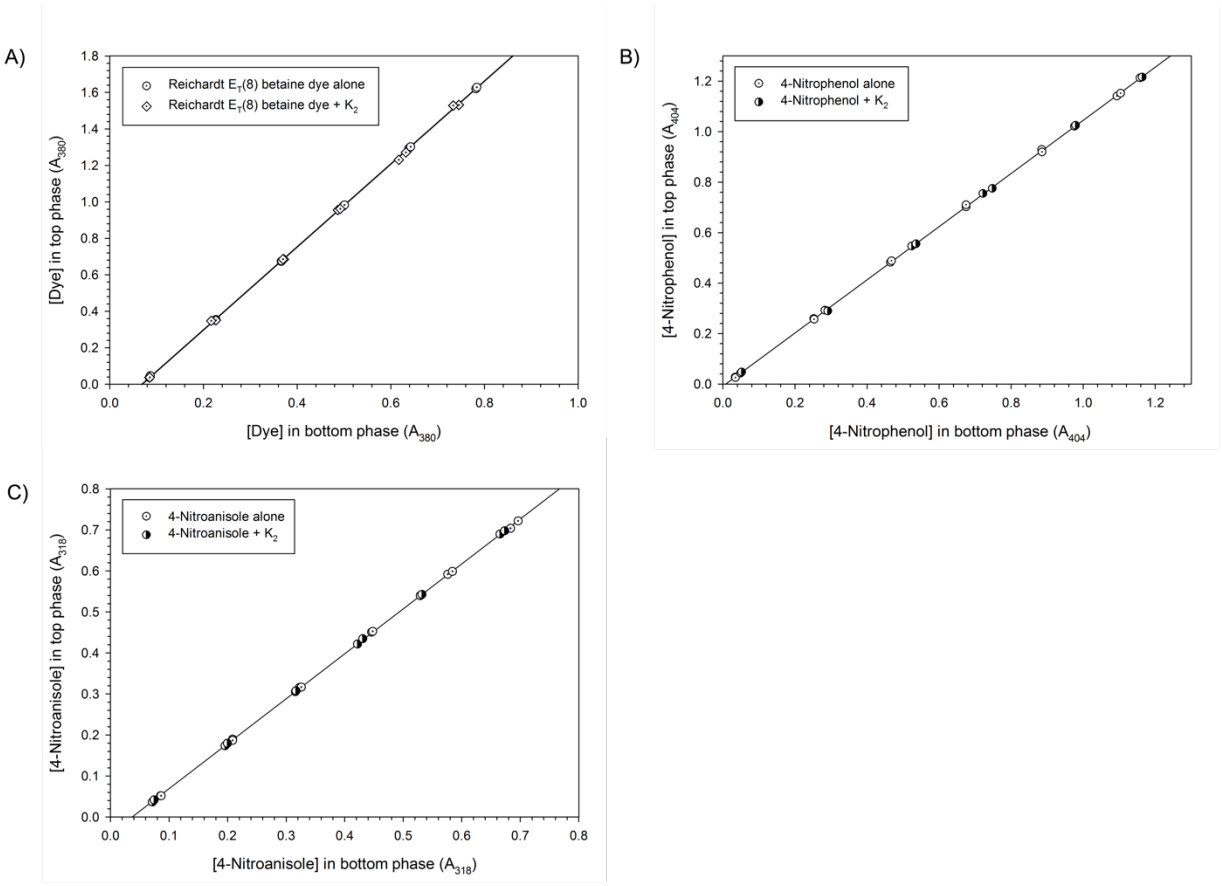

Figure S3. Dye distribution is unaffected by the presence of K_2. A) Concentration of the carboxylated Reichardt's betaine in the top and bottom phases of aqueous Ficoll-70/PEG-8000/0.01 M sodium phosphate buffer. B) Concentration of 4-nitrophenol in the top and bottom phases of aqueous Ficoll-70/PEG-8000/0.01 M sodium phosphate buffer. C) Concentration of 4-nitroanisole in the top and bottom phases of aqueous Ficoll-70/PEG-8000/0.01 M sodium phosphate buffer. The slopes of the linear curves represent the partition coefficient of each dye. The definition of the symbols is indicated in each panel.